Available online at www.sciencedirect.com

SciVerse ScienceDirect

Ceramics International 39 (2013) 7817–7829

CERAMICS INTERNATIONAL

www.elsevier.com/locate/ceramint

Large scale synthesis of non-transformable tetragonal Sc_2O_3, Y_2O_3 doped ZrO_2 nanopowders via the citric acid based gel method to obtain plasma sprayed coating

Mohammad Reza Loghman-Estarki[a,*], Hossein Edris[a], Reza Shoja Razavi[b]

[a]Department of Materials Engineering, Isfahan University of Technology, Isfahan, P.O. Box 84156-83111, Iran
[b]Department of Material Engineering, Malek Ashtar University of Technology, Isfahan, Shahin-shahr, Iran

Received 15 February 2013; received in revised form 11 March 2013; accepted 12 March 2013
Available online 26 March 2013

Abstract

Non-transformable tetragonal scandia, yttria doped zirconia (SYDZ) nanopowders were prepared in large scale by the citric acid (CA) based gel method. The effect of ethylene glycol monobutyl ether (EGM):CA ratios and pH on the structure, morphology and SYDZ particle size was investigated. The microstructure of SYDZ was characterized by XRD, Raman scattering, TG–DTA, SEM, TEM, and FTIR analyses. The SYDZ nanopowders, synthesized with $1Zr^{4+}$:4EGM:4CA mole ratio in acidic medium (pH ~1) at 700 °C, had an average diameter of 15 ± 2 nm. Finally, air plasma spray (APS) coatings were produced from nanostructured SYDZ agglomerated powders.

Keywords: A. Sol–gel; Zirconia based ceramics; Metastable tetragonal

1. Introduction

Zirconia based ceramics exhibit several crystalline modifications: monoclinic (m-phase), that is thermodynamically stable at temperatures below 1172 °C; tetragonal (t-phase), stable at the temperature range of 1172–2347 °C; cubic (c-phase), stable above 2347 °C; and rhombic, stable at a high pressure. Further, trivalent cation addition, especially Sc^{3+} and Y^{3+}, assures zirconia stabilization in the tetragonal structure at room temperature. This improves high temperature phase stability of zirconia and makes the stabilized ZrO_2 appropriate for use as high temperature thermal barrier coatings (TBCs) [1–5].

The applications of zirconia strongly depend on both crystal structure and phase transformations. The cubic phase of zirconia is a good candidate for SOFCs, oxygen sensors, electrochemical capacitor electrodes and ferrules due to its ionic, electrical [5–7] and optical [1] properties. Tetragonal zirconia can be used as an effective catalyst due to its unique amphoteric characteristics and redox properties [4]. The transformable tetragonal zirconia, such as yttria stabilized zirconia (YSZ) (called t-phase), is used as an engineering ceramic material due to its high values of strength and hardness. This hardening mechanism is due to the transformation of the tetragonal phase into the monoclinic phase, which implies a volume change associated with pseudoplasticity [5,8,9]. The 'non-transformable' metastable tetragonal YSZ phase (called t′) is remarkably resistant and does not undergo transformation to the monoclinic phase under stresses. The t′ phase is distinguishable by its antiphase domain boundaries and numerous twins [5,6]. This phase is widely used for thermal barrier coatings applications due to the formation of a tweed microstructure which tends to increase the thermomechanical performances. This microstructure corresponds to a three-dimensional pseudo-periodic lattice of high Y_2O_3 cubic particles within all of the t′ grains [5,6].

Recently, codoping zirconia with Al_2O_3, Sc_2O_3, Y_2O_3, Bi_2O_3, Sm_2O_3, Yb_2O_3, CeO_2, etc. has attracted researchers to improve thermal and electrical properties of this ceramic [10,11]. Yttria stabilized zirconia (YSZ) had a phase stability up to 1200 °C, but upon doping YSZ with scandium oxide (scandia, at specific content), the thermal stability of this ceramic was improved up to 1400 °C. Increasing the thermal

*Corresponding author. Tel.: +98 312 5225041; fax: +98 312 5228530.
E-mail addresses: loghman57@gmail.com, mr.loghman@ma.iut.ac.ir (M.R. Loghman-Estarki).

0272-8842/$ - see front matter © 2013 Elsevier Ltd and Techna Group S.r.l. All rights reserved.
http://dx.doi.org/10.1016/j.ceramint.2013.03.042

stability of zirconia ceramics can have high potential applications in improving the efficiency and performance of engine [5,11]. The Y_2O_3–Sc_2O_3–ZrO_2 system with 8–12 mol% stabilizing content has been studied by Irvine's group [12]. They showed that a higher conductivity could be obtained with SYDZ than YSZ and scandia stabilized zirconia (ScSZ). Furthermore, alternative materials to YSZ for improving TBCs life time are being sought. One approach was taken by Jones [13] who sought to combine the stabilizing efficiency of Y_2O_3 with the vanadate-corrosion resistance of Sc_2O_3. Jones showed that the most effective stabilizer composition for ultra high temperature TBCs was probably near 90–95% Sc_2O_3 and 10–5% Y_2O_3 [5,13]. Jang [14] reported that the amount of tetragonal phase was increased by codoping with scandia and yttria. This was due to the lower stabilization of zirconia by scandia [10,14]. The strength of the codoped material was about 10% higher than that of the reference material (YSZ and ScSZ) [10]. It was also reported that a higher fracture toughness of the codoped material was obtained, as compared to the reference material, in accordance with the higher tetragonal phase content and the resulting enhanced transformation toughening [10,14].

The rare earth stabilized zirconia (RESZ) nanostructures have received increasing interest in recent years [3,6–8]. The traditional method of preparing multicomponent zirconium oxides involves initial mechanical mixing of oxide powders and then high temperature calcination to homogenize the metal oxide–zirconia composition via solid state reactions. Serious problems in processing zirconia-based solid solutions resulted from these high-temperature techniques, including uncontrolled grain growth, deep segregation of dopant and possible loss of stoichiometry due to the volatilization of a reactant at high temperatures [9]. For this reason, based on wet chemical routes, several increasingly important alternatives make the synthesis of zirconia-based solid solutions at mild temperatures possible. In order to prepare multidopant zirconia nanocrystals such as ScSZ (Sc_2O_3 doped ZrO_2), YSZ (Y_2O_3 doped ZrO_2) and SYDZ, several methods such as co-precipitation, alkoxide and the acetic acid based gel, hydrothermal process and gel combustion process (such as citrate–nitrate and glycine–nitrate route) are well-known [15–21].

One promising method is the citric acid based gel preparation method (i.e. the polymerized complex based on the Pechini method), which relies on the formation of complexes of alkali metals, alkaline earth metals and transition metals, or even nonmetals with bi- and tridentate organic chelating agents such as citric acid (CA) [19,20]. A polyalcohol such as ethylene glycol (EG) is added to establish the linkages between the chelates by a polyesterification reaction, resulting in the gelation of the reaction mixture. By calcinating the gel, nanocrystalline powder was obtained [22,23]. Such kind of preparation enabled us to obtain homogeneous, transparent, and very stable polymeric sols. It is very cheap and holds a number of advantages over the popular but rather expensive sol–gel synthesis via alkoxide route. The sols produced via the polymer route may also be good candidates for the preparation of thin, dense yttria–scandia zirconia films for thermal barrier coatings and in intermediate temperature, solid oxide fuel cells (SOFC) [20,21].

According to the experiment described here, we aimed to obtain a large amount of SYDZ nanopowders using the citric acid based gel method. In this approach, the effect of pH and EGM:CA ratios on the structure, morphologies and the particle size of SYDZ was investigated. Moreover, the majority of works used Sc_2O_3 as a stabilizer to obtain cubic phase of zirconia due to its electrical properties [5,19,20], but in this case, t′ phase of zirconia was aimed at. To this end, Sc_2O_3: Y_2O_3 ratios were changed to obtain t′ phase of zirconia. This phase can be used in high temperature TBCs. Finally, the suspensions of these nanopowders were spray dried to obtain APS coating.

2. Experimental

2.1. The synthesis of SYDZ nanopowders

Zirconium oxychloride octa hydrate (98.5% pure) and yttrium nitrate (99.8% pure) were purchased from Rekhim (Russia Company) and scandium nitrate was prepared from Tropimetals International Limited Company (China) with 97.86% purity. Other chemicals used in our experiments such as citric acid monohydrate and ethylene glycol monobutyl ether (EGM) were bought from Merck Company. Both of these materials were of analytical grade and used as received without further purification.

In a typical experiment, 3 g $ZrO(Cl)_2.8H_2O$, $Sc(NO_3)_3.6H_2O$, and $Y(NO_3)_3 \cdot 6H_2O$ (i.e. 90% mol Sc_2O_3 and 10% mol. Y_2O_3 as a dopant) and citric acid monohydrate ($C_6H_8O_7 \cdot H_2O$) were dissolved in deionized water, and different amounts of ethylene glycol monobutyl ether (EGM) were then added to form a sol at 50 °C for 1 h (Table 1). A white solution was obtained and further heated at 80 °C for 1 h to remove excess water. During continued heating at 140–150 °C for 1 h, the solution became more and more viscous, finally turning into a xerogel. To complete drying, the xerogel was placed at 250 °C for 1 h. The resultant powder was a precursor. In the furnace, the precursor was calcined at 700 °C for 2 h, in an alumina boat; then it was cooled to reach the room temperature. To investigate pH effect on the morphology and phase structure, in parallel reactions series, pH value was changed from 1 (acidic medium) to 7 (neutralized medium) and 9 (alkali medium) by adding adequate liquor ammonia (for

Table 1
Number of samples and their corresponding preparation conditions.

Sample no.	EGM:Zr^{4+} mole ratio	CA:Zr^{4+} mole ratio	pH	Calcination temperatures (°C)	Calcination time (h)
S1	1.2:1	1:1	1	700	2
S2	4:1	4:1	1	700	2
S3	EG:Zr^{4+}=4:1	4:1	1	700	2
S4	4:1	4:1	7	700	2
S5	4:1	4:1	9	700	2
S6	4:1	4:1	9	800	2
S7	4:1	4:1	9	1000	2

changing the pH of precursor, 13 and 23 ml of the concentrated ammonia was added, so the final pH of solution was adjusted to 7 and 9) and other parameters such as EGM:CA ratio, and calcination temperature were kept constant. The number of samples is summarized in Table 1.

2.2. The APS coating setup

The agglomerated nanopowder was thermally sprayed using an air plasma spray (APS) torch (Plasma-Technik A3000S system, gun: F4-MB, Sulzer Metco, Wohlen, Switzerland). The deposition was made using argon and hydrogen as plasma-forming gases. Inconel 738LC Ni-based super alloy was used as the substrate material. In order to enhance the adhesion of the coating and obtain a sharp-peaked surface contour, the substrate was first blasted with alumina grit and then cleaned with acetone. Commercially Ni–22Cr–10Al–1Y (wt%) powder (22 SN 6883, S.N.M.I.-Avignon) as a feedstock for bond coat was atmospheric plasma sprayed by the Plasma-Technik A3000S system with an F4-MB plasma torch (Sulzer Metco AG, Winterthur, Switzerland). The bond coat powders were sprayed based on the standard parameters recommended by the Sulzer Metco (Ar flow = 65 slpm, H_2 flow = 14 slpm, arc intensity = 600 amper (A), spraying distance = 120 mm, spraying velocity = 1000 mm/min, anode nozzle internal diameter = 6 mm, and feedstock feed rate = 40 g/min). The parameters used to spray the nanostructured SYDZ coating were developed internally (Ar flow = 35 slpm, H_2 flow = 10 slpm, arc intensity = 600 Å, spraying distance = 120 mm, spraying velocity = 1000 mm/min, anode nozzle internal diameter = 6 mm, and feedstock feed rate = 18 g/min).

2.3. Characterization equipment

XRD patterns (X'Pert Pro, Philips, Holland) were recorded by a Rigaku D-max C III, X-ray diffractometer using Ni-filtered Cu K_α radiation ($\lambda = 1.5406$ Å), generator setting 40 kV and 30 mA and step size 0.05. Field emission scanning electron microscopy (FESEM) images were obtained on S-4160 (Hitachi Ltd., Japan). Transmission electron microscopy (TEM) micrographs were obtained on a Philips EM208 transmission electron microscope with an accelerating voltage of 100 kV. Micro-Raman system (LabRaman Almega Thermonicolet) with a laser ($\lambda = 785$ nm) as the excitation source and an Olympus BX-41 optical microscope was utilized to collect the spectra of the samples. Fourier transform infrared (FT-IR) spectra were recorded on a JASCO 680 plus spectrophotometer in KBr pellets. TG/DTA analysis was carried out using a simultaneous thermal analysis instrument (NETZSCH STA 409 PC/PG) with a flow rate of 20.0 ml min^{-1} and a heating rate of 10 °C min^{-1}. Analysis of particle size was done with the Scion image Beta 4.02 software for image processing.

The crystallite sizes ($\boldsymbol{D_{(101)}}$) were calculated from the line broadening of the X-ray diffraction peaks at $2\theta = 30.5°$ (hkl = (101)) using the Scherrer equation (Eq. (1)) [1,23,24]

$$D_{(101)} = k\lambda/\beta\cos\theta \quad (1)$$

where β is the breadth of the observed diffraction line at its half-intensity maximum, k is the so-called shape factor, which usually takes a value of about 0.9, and λ is the wavelength of X-ray source used in XRD.

3. Results and discussion

3.1. Thermal behavior of precursor (gel)

Upon heating the solution containing zirconium oxychloride, yttrium and scandium nitrate, citric acid, and EGM are transformed into a semi-solid black colored gel type of mass, which by further heating, swells up to yield a foamy charred mass. Fig. 1a shows the results of differential thermal analysis (DTA) and thermogravimetric (TG) analysis for the SYDZ precursor (prepared with $1Zr^{4+}$:4EGM:4CA). The DDTA spectra (the second derivative of DTA) show the nature of reactions better than the DTA one. The endothermic peak in the DDTA curve around 110 °C, corresponding to the first weight loss shown by TG/DTA curve, is due to the dehydration of the precursor. The endothermic peak in the DDTA curve around 200 °C, corresponding to the second small weight loss shown by TG curve, can be ascribed to the evaporation of any excess ethylene glycol monobutyl ether (b.p. 199 °C) in the gel [25]. The exothermic peak in the DDTA curve around 400 °C is due to the carbonization or bond breaking of organic moieties in the precursor together with the evolution of great amounts of gases such as CO_2 [26]. According to DTG analysis (green line, Fig. 1b), the third weight loss step occurs at the temperature range of 395–600 °C. This weight loss was attributed to the burning out of organic species in the powder precursor and decomposition into scandia–yttria doped zirconium oxides (SYDZ) [25,26]. The strongest exothermic peak around 591 °C in the DTA curve can be primarily associated with the crystallization of amorphous gel [25–27]. Based on TG/DTA analysis (Fig. 1), the initial calcination temperature was 600 °C, but when the sample was calcined at 600 °C, coaly powder was obtained which showed that there was still some small carbon that remained on the sample. So, the calcination temperature was selected to be 700 °C for 2 h. This was confirmed through calcination experiments because the powder, calcined at a temperature greater than 600 °C, became white. XRD patterns (Fig. 2a) also showed that low calcination temperature (600 °C) was not sufficient for the formation of the solid solution between Sc_2O_3, Y_2O_3 and ZrO_2, resulting in tetragonal crystal structure.

Raisi group report [3] the thermal behavior of the YSZ gel prepared with $1Zr^{4+}$:4EG:4CA mole ratio using the conventional Pechini method. The total weight loss, which was about 85% of the total precursor mass, occurred in several steps. The first weight loss occurred at about 250 °C that corresponded to the first endothermic peak shown by the DTA curve. It was due to the evaporation of water and any excess ethylene glycol (b.p. 168 °C) in the gel [3,26]. The second weight loss, shown by TGA curve around 250–480 °C, can be ascribed to the decomposition of the organometallic compounds that were formed by hydrolysis

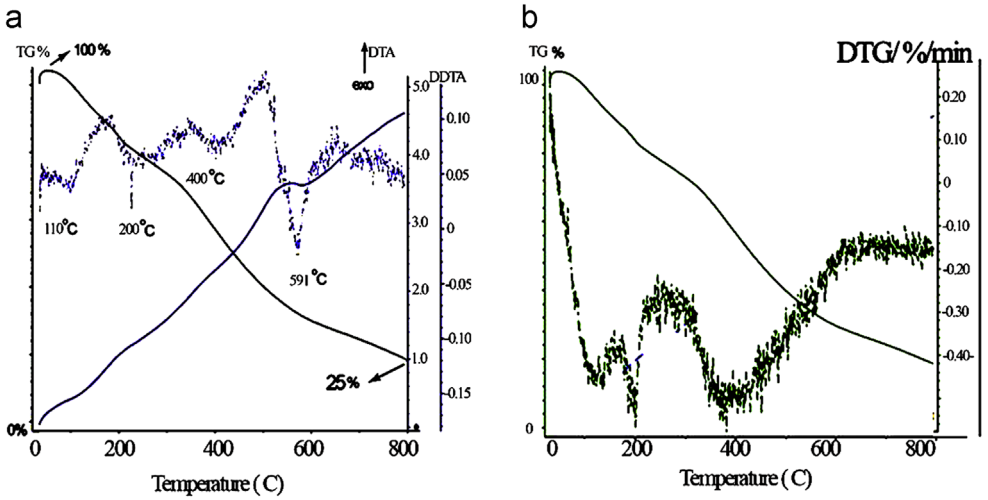

Fig. 1. (a) TG/DTA, (b) TG/DTG spectra of SYDZ precursor (gel) prepared by the modified Pechini method (a and b). (For interpretation of the references to color in this figure, the reader is referred to the web version of this article.)

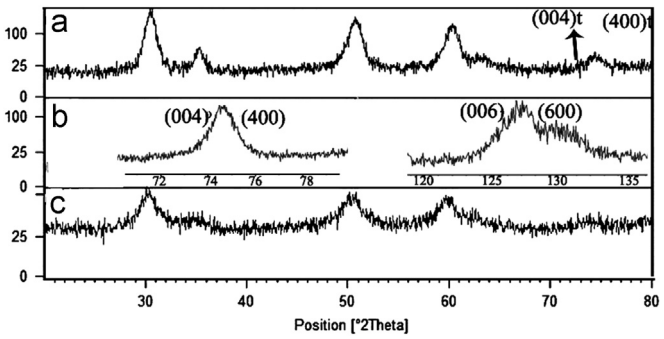

Fig. 2. XRD patterns of SYDZ nanopowders synthesized at different condition (a) EGM: Zr^{4+}=CA: Zr^{4+}=4:1, 600 °C/2h. (b) EGM: Zr^{4+}=CA:Zr^{4+}=1.2:1, 700 °C/2h, (c) EGM: Zr^{4+}=CA : Zr^{4+}=4:1, 700 °C/2h.

and condensation of the precursor gel [19]. The third weight loss step, corresponding to the second exothermic peak at 440 °C, which was shown by DTA curve, occurred at the temperature range of 480 -580 °C. The weight loss at this step might be attributed to the carbonization or bond breaking of residue organic moieties in precursors [19,21,26]. Above 580 °C, no significant thermal events were perceived suggesting that all organic components were decomposed [3].

3.2. The phase determination of products

Fig. 2 shows the XRD patterns of the products at different conditions. As can be seen in Fig. 2a, when the sample was calcined at 600 °C/2 h, the crystallization of the products was not completed. Upon increasing the calcination temperatures to 700 °C/2 h, the crystallinity of the products was improved (Fig. 2b,c). Fig. 2b and c shows the XRD patterns of as-synthesized powders prepared at different mole ratios of EGM to CA. The distinguishing peaks for the tetragonal (t) phase of SYDZ occurred at $2\theta = 30.5^\circ$, 35.2°, 50.3° and 60.02° for (101), (110), (200) and (211) reflections, respectively. So, all XRD patterns of the as-prepared sample, calcined at 700 °C, were indexed as a tetragonal (t) phase. This is very close to other studies (JSPDS no. 01-071-1284, space group $P4_2/nmc$) [5,28]. The calculated values of a and c parameters were equal to 0.35984 nm and 0.50105 nm, respectively. No impurity such as Y_2O_3, Sc_2O_3, etc. was found in X-ray diffraction patterns. These results showed that Y_2O_3 and Sc_2O_3 were successfully doped in zirconia lattice using the citric acid based gel preparation method. The distinguishing peak for t phase occurred at $2\theta = 30.5^\circ$ for (101) reflection, and the respective peaks for monoclinic (m-phase) occurred at $2\theta = 28.4^\circ$ and $2\theta = 31.6^\circ$ for (111) and (−111) reflections [3,4]. So, the presence of m-phase of zirconia can be ruled out based on the absence of characteristic peaks of m-phase in all XRD patterns of the as-prepared sample.

The crystallites size of products (D_{101}, determined from the line broadening in the XRD patterns) synthesized from the modified Pechini method at 700 °C/2 h has been shown in Table 2 along with certain literature data obtained from the classic Pechini method [3,19,20,26]. The results show that the crystallites sizes of all samples are approximately the same. The difference between the present work and other similar works was in the small particle size of the product and reduction in reaction time from 24 h to 5 h, as will be discussed later.

It should be noted that all samples prepared above were made with a Sc_2O_3:Y_2O_3 mole ratio equal to 3.6:0.4%. As mentioned before, the t' phase was obtained at a specific amount of stabilizer agent. To this end, the amount of Sc_2O_3: Y_2O_3 mole ratios was changed and the SYDZ nanopowders were sintered at 1400 °C. It should be noted that in order to clearly observe the tetragonal splitting in the entire 2θ region in yttria-containing zirconia ceramics, the material must be sintered above 1100 °C. Below 1100 °C, the 2θ angle, at which tetragonal reflections occur, becomes a function of a number of parameters, such as the change in composition, different thermal treatments, the variation of lattice parameters with a change in composition, etc [29]. Fig. 3 shows the SEM

Table 2
The crystallite size of as-prepared product and comparison with other similar works.

Stating materials	Reaction time, calcin. temp.	Particle size (nm)	Crystallite size (nm)	Ref.
$ZrCl_4$, $Y(NO_3)_3$, 4EG, 4CA	24 h, 650–800 °C	90–100	7–10	[3]
$ZrO(NO_3)_2$, $Y(NO_3)_3$, $Sc(NO_3)_3$, 1.41CA, NH_3	24 h, 800 °C	13.5–23.3	–	[19]
$ZrO(NO_3)_2$, $Y(NO_3)_3$, $Sc(NO_3)_3$, 1.41CA, NH_3	24 h, 800 °C	12.1–16.3	–	[20]
$ZrOCl_2 \cdot 8H_2O$, Y_2O_3, HNO_3, liquor ammonia, 2.3CA	24 h, 650–800 °C	20–30	11	[26]
$ZrOCl_2 \cdot H_2O$, $Y(NO_3)_3$, $Sc(NO_3)_3$ Water, 1TM:4EGM:4CA	5 h, 700 °C	~15	11.95	Present work

images of sintered SYDZ samples at 1400 °C with different Sc_2O_3: Y_2O_3 mole ratios. Our current research [17] shows that, at Sc_2O_3:Y_2O_3 mole ratio equal to 3.6:0.4 mol%, t' phase was obtained. This tetragonality is within the range of $c/a\sqrt{2} = 1.0025–1.0075$ as cited in Refs. [2,5]. So, the phase stability of SYDZ samples at 1400 °C and the splitting of (004)/(400) at 2θ=74–76° confirm that a nontransformable tetragonal phase is produced by 4 mol% Sc_2O_3,Y_2O_3 doped ZrO_2.

It is worth noting that the assignment of cubic and tetragonal structures, based solely on the x-ray diffraction analysis, can be difficult because the cubic and tetragonal structures (a=0.5124 nm for cubic, and a=0.5094 nm and c=0.5177 nm for tetragonal structures) are very similar [29]. However, these split Bragg peaks from the tetragonal phase in zirconia overlap with one another due to the particle size broadening [30]. Raman spectroscopy is more suitable in distinguishing different modifications of the stabilized zirconia crystal structure [29–31]. It is due to the higher sensitivity of the Raman scattering to both intermediate periodicity and oxygen displacement in comparison with the XRD [4,31]. According to group theory, the monoclinic, tetragonal and cubic phases of zirconia are expected to have 18 (9Ag+9Bg), 6($1A_{1g}$+$2B_{1g}$+$3E_g$) and $1T_{2g}$ Raman active modes, respectively [4]. Fig. 4 shows the typical Raman spectra of the as-obtained product prepared with 1TM:4CA:4EGM sintered at 1400 °C, using the laser at λ=785 nm. The peaks centered at 149.25 (corresponding to E_g mode), 259.45 (E_g mode), 322.80 (B_g mode), 460.01 (E_g mode), 620.16 (B_g mode) and 639.96 cm^{-1} (A_g mode), confirming that the tetragonal phase of as-obtained SYDZ was obtained. The assignment of the Raman modes is done according to Refs. [11,31]. This is in agreement with our X-ray analysis (Fig. 3c). It is worth noting that the six Raman frequencies of t-zirconia in different literatures are in the range of (i) 131 (E_g mode)–155 (B_{1g}), (ii) 240 (E_g)–266 (A_{1g}), (iii) 290 (B_{1g})–330 (E_{1g}), (iv) 410 (E_{1g})–475 (E_g), (v) 550 (A_{1g})–615 (B_{1g}), and (vi) 616 (E_g)–645 [4,11,31]. The presence of m-ZrO_2 can be ruled out based on the absence of peaks at 102, 179 and 381 cm^{-1} [4], which are supposed to be the strong peaks for m-ZrO_2.

3.3. The morphologies and particle size of products

The effects of mole ratios of ethylene glycol monobutyl ether (EGM) to citric acid (CA) in the starting solution on the morphology and particle size of samples are shown in Fig. 5. According to Fig. 5a, when Zr^{4+}:EGM:CA mole ratio was 1:1.2:1, the as-formed products consisted of a large irregular shape with submicrograins (~110 nm diameter, inset Fig. 5a).

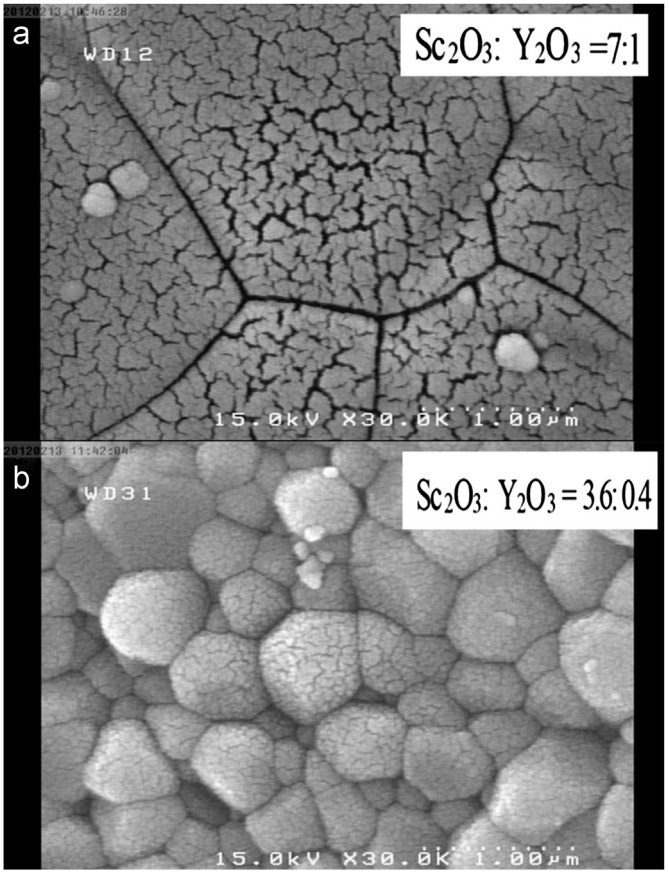

Fig. 3. SEM images of sintered SYDZ nanopowders synthesized at different Sc_2O_3: Y_2O_3 mole ratio percent (a) 7:1 (b) 3.6:0.4.

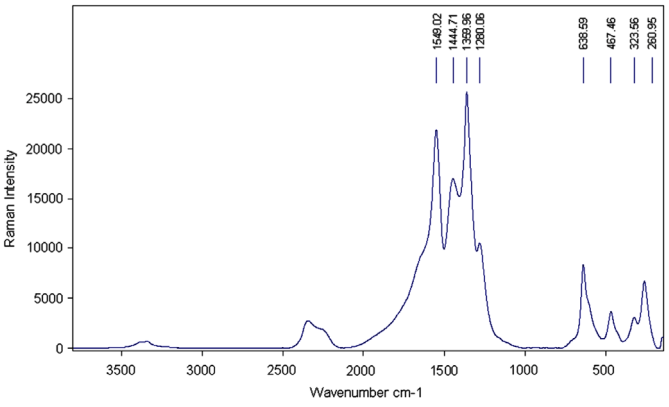

Fig. 4. Ramanscatteringof sintered SYDZ prepared with 1TM:4CA:4EGM at 700 °C/2 h.

Upon increasing the Zr^{4+}:EGM:CA mole ratio to 1:4:1 (Fig. 5b), nanoparticles with 24–34 nm diameters were obtained, while in the presence of ethylene glycol (conventional Pechini method) (Fig. 5c), the nanocrystals with an average diameter of 70–90 nm were obtained. A close look at Fig. 5c shows that more agglomerated particles were formed in comparison to Fig. 5b. These results are consistent with those obtained by TEM analysis, to be discussed later. For rare earth stabilized zirconia, similar works were done by Roberts' groups [32,33]. In their works, CA:EG (ethylene glycol) mole ratios varied from 0.6 to 2.4 to obtain nanopowders with less porosity and agglomerates. The optimized CA:EG mole ratio was 2.4 ($CA:Zr^{4+}=EG:Zr^{4+}=4.77$) and the particle size of the obtained powders was 10–20 nm, as calcined at 325–400 °C for 6 h. Furthermore, in other similar works by Raissi group [3], the agglomerated size of YSZ powder was 90 nm with $EG:Zr^{4+}=CA:Zr^{4+}$, which was equal to 4:1, as calcined at 650 °C/2 h. Another work on ceria stabilized zirconia (CSZ), using the conventional Pechini method ($CA:Zr^{4+}=1.8$), was done by Rezaei group [34]. The crystallite size of CSZ varied from 15.8 to16.7 nm by increasing CA:EG from 2:1 to 10:1 at the calcination temperature of 700 °C/2 h. Furthermore, Costa [27] also obtained scandia stabilized zirconia (ScSZ), which mainly consisted of hard agglomerates exhibiting irregular shapes with faceted borders that had an average size of around 20 μm. However, these hard agglomerates consist of sintered nanoparticles resulting from the high-energy environment during thermal decomposition of the large amount of organic compounds used in the synthesis of the polymeric precursors. They used the conventional Pechini method with $1Zr^{4+}$:4CA: 16 EG at 500–650 °C/4 h. However, in the present work, the average agglomerated size was 30–40 nm and it consisted of primary particles with ~15 nm diameters, as obtained by $EGM:Zr^{4+}=4:1$ at the calcination temperature of 700 °C for 2 h (see TEM image in Fig. 6a). So, in our case, the average size of agglomerate was less than that in the conventional Pechini method [3,32,33].

To ensure the compositional homogeneity of metal ions and the fuel for combustion during calcinations, citric acid is the complexing agent for the two chemical synthesis techniques (conventional Pechini and the present work). The oxygen in the reaction atmosphere is the oxidizer for the combustion. Therefore, the exothermic reactions of the oxidative removal of organic compounds during calcinations at relatively high temperatures (700 °C) often transform the weak bonds between particles into sintered necks, producing undesirable agglomeration of the powders. The difference in the distribution of the agglomerate size of powders produced by following the two chemical synthesis techniques is due to the different (organic compounds)/(powder) ratios. Therefore, additional quantities of organic compound (from Zr^{4+}:EGM:CA mole ratio 1:1.2:1 to 1:4:4) produce enough energy to join the particles together during calcination, resulting in agglomerates. The degree of agglomeration of powders, obtained by the polymeric precursor technique (conventional Pechini method), is higher than that of powders obtained by the present work due to the relative higher quantities of organic compound used in the former synthesis technique. Therefore, the formation of agglomerates can be a problem when synthesizing ceramic materials. In Section 3.7, more detailed discussion on the advantage of the present work using the conventional Pechini method will be presented. It is noticeable that the pH of the above solutions was ~1. These experimental results show that the mole ratio of ethylene glycol to citric acid is a key factor

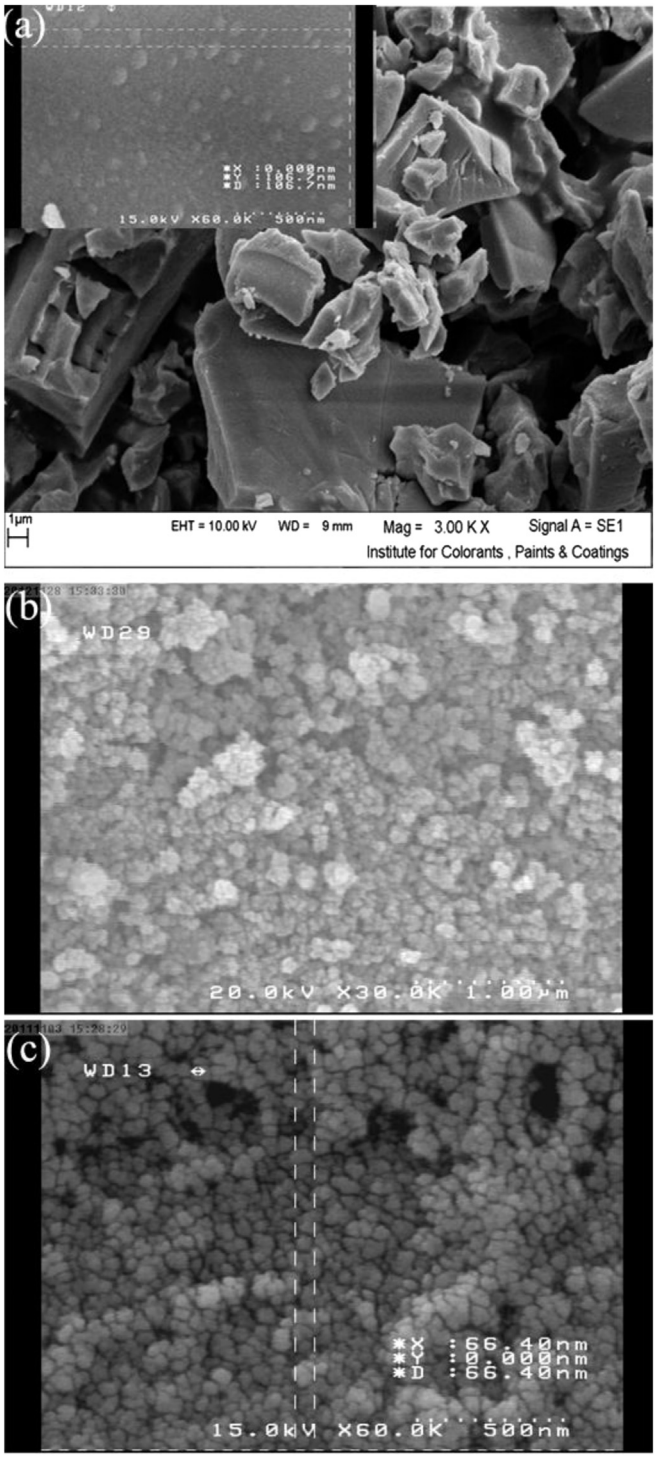

Fig. 5. SEM images of SYDZ nanoparticles with EGM:CA:TM of (a) 1.2:1:1, (b) 4:4:1and(c)EG:CA:TM(1/4)4:4:1 (conventional Pechini method).

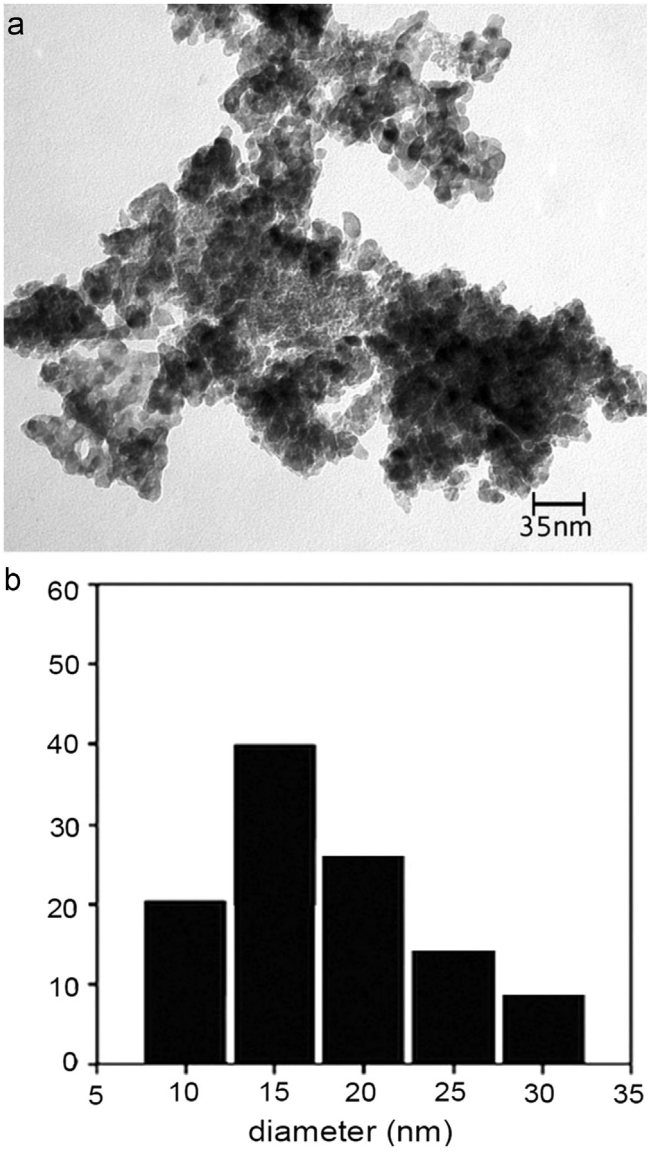

Fig. 6. TEM images of SYDZ nanopowders prepared at 700 °C for 2 h (a) with 1TM:4EGM:4CA, TM=transition metal (b) Size distribution of SYDP samples obtained by measuring random 40 size of nanoparticle.

for the changing size of SYDZ powder by the citric acid based sol–gel process.

Typical TEM image of SYDZ nanoparticles is shown in Fig. 6. TEM micrographs clearly indicate that the particle sizes of synthesized powders are in the nano-range and the particles, even when agglomerated, consist of fine grains. From the TEM images (Fig. 6a), the average particle size for the powder, formed by Zr^{4+}:EGM:CA mole ratio 1:4:4 and calcined at 700 °C, could be estimated to be 15 nm (see Fig. 6b), whereas identically calcined powder, made with EG addition ($1Zr^{4+}$:4EG:4CA, conventional Pechini method), had an average particle size of 40–50 nm (see Ref. 17). As can be seen in Fig. 6a, particles are sintered together and most of them are slightly irregular. From the SEM (Fig. 5b) and TEM (Fig. 6a) images, it can be clearly observed that the degree of agglomeration is low in the synthesized powder, which has strong technological importance. So, these results confirm the importance of EGM as a key factor for controlling the agglomeration degree of nanocrystals. These results of TEM (Fig. 6a and b) analysis are in good agreement with XRD (Fig. 2; Table 2) analysis.

3.4. The effect of pH

The effects of pH on the morphologies and particle size of samples in the starting solution are shown in Fig. 7. The scanning electron microscopy images show a clear change in the morphology as the pH of solution was increased from 1 (Fig. 5b) to 7 and 9 (Fig. 7a–c). The particle morphology was changed from semi-spherical structures (observed at low pH ~1) to a flat facet that had desegregated fine particulates with ~100 nm diameters on its surface (observed at pH 7, Fig. 7a and b). Upon increasing pH to 9, dense agglomerated particles at a calcination temperature of 700 °C (Fig. 7b) were obtained. With increase in the calcination temperature of the sample prepared at alkaline pH from 700 °C to 1000 °C, it was seen that dense agglomerated particles were broken into semispherical particles with 90 nm diameters (Fig. 7c).

Fig. 8 shows TG–DTA plots obtained for the dark gel at alkali pH (pH=9). According to Fig. 8, the total weight loss was about 53% of the total precursor mass, occurring in two steps. The first weight loss occurred at about 115.2 °C, which corresponded to the evaporation of the adsorbed water. The second weight loss step occurred at the temperature range of 300–600 °C. The weight loss at 300–600 °C may be ascribed to the decomposition of organic compound [19,26]. The DTA plot, as depicted in Fig. 8, showed one endothermic peak at 115.2 °C, which was attributed to the evaporation of water, while in acidic medium, two endothermic peaks, corresponding to the evaporation of water and excess EGM, were observed (Fig. 1b). This result showed that at high pH, the total of EGM reacted with CA molecules [35,36]. The exothermic peak at 400 °C was associated with polymer charring and the elimination of organic species. The three endothermic peaks between 400 and 800 °C were related to free (unreacted with CA molecules) zirconium, scandium and yttrium salts in the dark gel [26].

For the pH 7 precursors (Fig. 9a), the sample calcined at 700 °C for 2 h was also composed of t-phase of SYDZ (JSPDS no. 01-071-1285, 0.35981 nm and 0.50103 nm, space group $P4_2/nmc$). But the peak height intensity of the main reflection of SYDZ was twice stronger than that of pH 9. The XRD patterns, obtained on the pH 7 and 9 precursors and heated at 700 °C for 2 h, are similar, as compared to Figs. 2 and 3b (pH=~1), except that the relative intensities of product are much higher. It is due to the different size of particles in which at pH 1, the very fine particles (~24–34 nm) caused peak broadening and X-ray diffraction intensities were lower than those of the sample synthesized at alkali pH (pH=9) with diameters being more than 100 nm.

The effect of pH on the formation of product can be described in terms of different stability constants of the M–CA complex (M=metal) under different pH values. The citric acid is a tribasic acid that can be dissociated in aqueous solution to $C_6H_7O_7^-$, $C_6H_6O_7^{2-}$ and $C_6H_5O_7^{3-}$ based on the pH

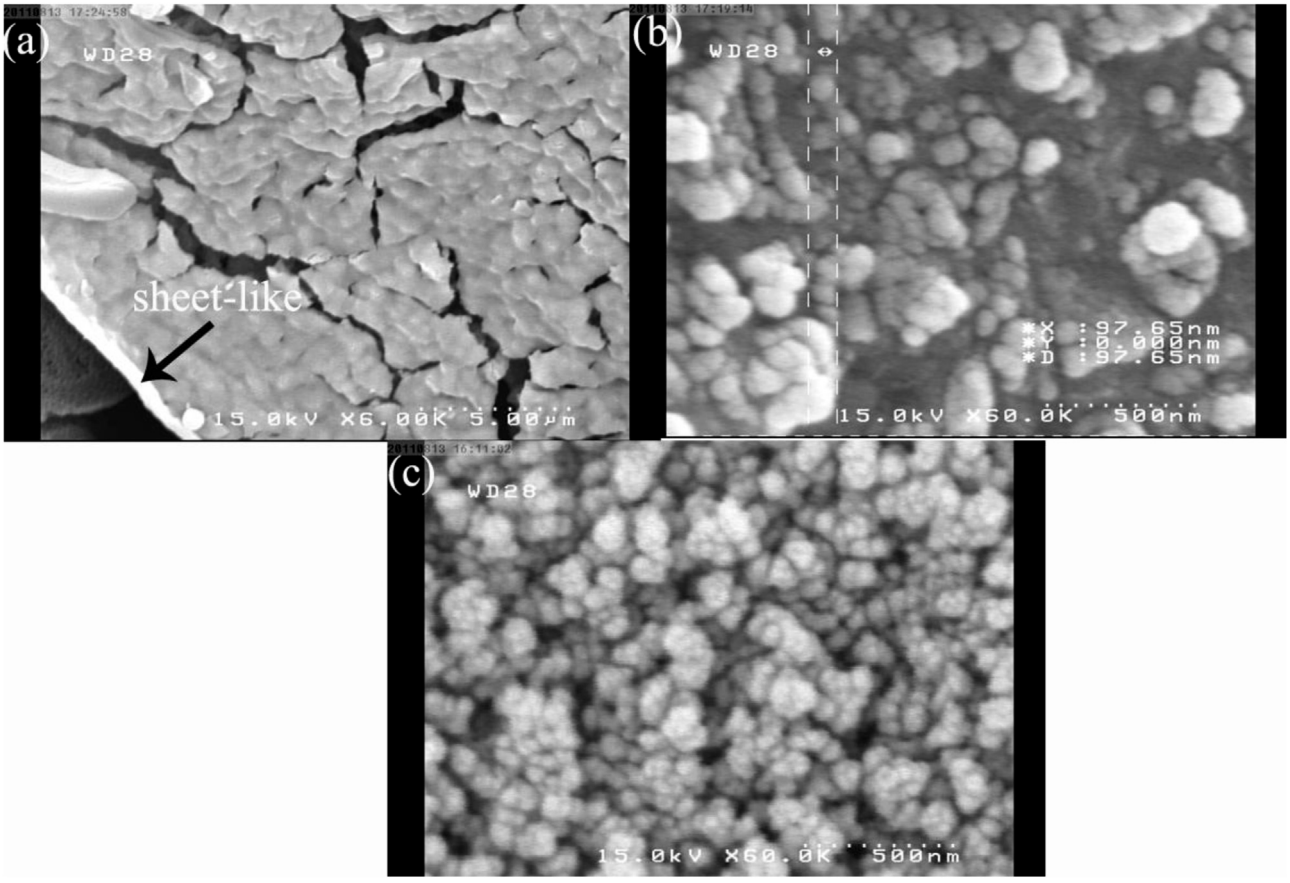

Fig. 7. SEM images of sample prepared by the modified Pechini method with 1TM:4EGM:4CA,TM=transition metal at different pH:(a) SYDZ, pH=7, at 700 °C/2 h; (b) SYDZ, pH=9, at 700 °C/2 h and (c) YSZ, alkaline pH,1000 °C/2 h.

of solution. In the present work, at low pH (pH=~1.0), $C_6H_7O_7^-$ is the prevailing species which can interact with M^{n+} ($M=Zr^{4+}$, Sc^{3+}, Y^{3+}) to form complex $M(C_6H_7O_7)^{n-1}$ [37,38]. At high pH (pH=~6.0), $C_6H_5O_7^{3-}$ becomes the predominant species which can interact more strongly with M^{n+} to form stable complex $M(C_6H_7O_7)^{n-3}$. According to the stability constant for the above reaction, it seems that calcinations temperature ranges of 700–800 °C were not sufficient for breaking the complex $M(C_6H_7O_7)^{n-3}$ formed at pH 9. Upon increasing calcination temperature to 1000 °C, the aforementioned complex was broken and nanoparticles with 90 nm diameter were obtained (Fig. 7c). At acidic pH, low calcinations temperature was required for the formation of SYDZ nanoparticles in comparison to the basic pH. It was due to the low stability constant of $M(C_6H_7O_7)^{n-1}$ formed at pH~1. It should also be noted that some researchers have also used an acidic environment (low pH medium) for synthesizing nanocrystals via the Pechini method. The advantage of using lower ratio of citric acid to metal ions was that the acidic pH was enough to ionize the total amount of $[COOH]^-$ for chelation [39–42].

3.5. The FTIR of the as-prepared samples

Fig. 9 shows the FT-IR spectra of the precursor and the as-synthesized products in the range of 400–4000 cm^{-1}. The precursor (xerogel), prepared in acidic medium (pH=1), showed the characteristic absorption bands at about 3434.6, 2923.56 1728.87 and 1638.23 cm^{-1}, corresponding to the –OH group, $–CH_2$, symmetry and asymmetry carboxyl group vibrations, respectively (Fig. 9c), while in alkali medium (Fig. 9b), in addition to –NH group (3208.97 cm^{-1}), the same functional group could be seen. The wave number difference ($\Delta\nu$) between the antisymmetrical and symmetrical stretching modes of –COOH groups in the acidic and alkali gels was 90.64 and 325.91 cm^{-1}, respectively. For pure sodium citrate, $\Delta\nu=175$ cm^{-1}, which was much smaller than 325.91 cm^{-1}. Thus, a unidentate complex was formed by the coordination of citric acid with metal ions in the alkali gel, while bidendate complex was obtained in the acidic gel ($\Delta\nu=90.64<175$ cm^{-1}) [19,20].

In the FT-IR spectrum of the as-synthesized sample at 700 °C (Fig. 9c,d), there were four spectroscopic bands at around 3421–3434.6, 2922–2924, 1728.87, 1618–1638.23 cm^{-1} and ~442–462 cm^{-1} which correlated to the hydroxyl group, $–CH_2$, C=O [18,39] and Zr–O–Zr bond [6,19], respectively. These peaks confirmed that a small amount of citric acid existed in the as-prepared sample. These small amounts of citric acid stabilized SYDZ nanostructures [6,18,39]. FT-IR spectroscopy was also a highly effective technique for the determination of crystal phase of zirconia [42–47]. From a group theory analysis, m, t and c

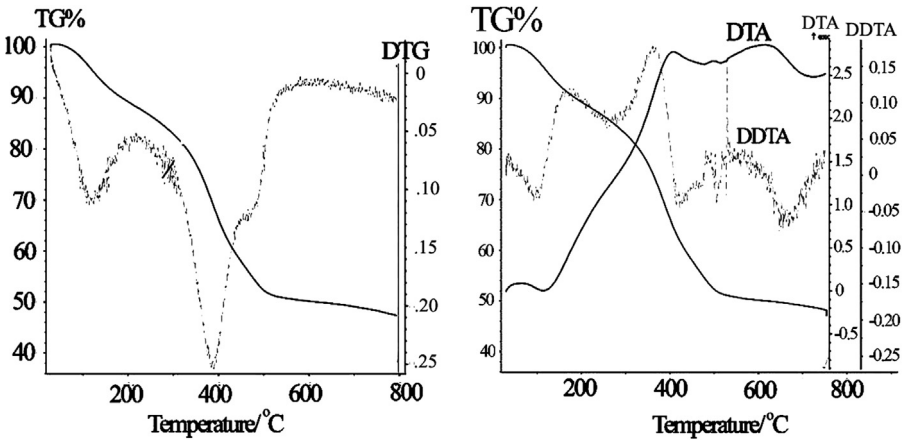

Fig. 8. TG/DTA analysis of SYDZ gel in alkali medium.

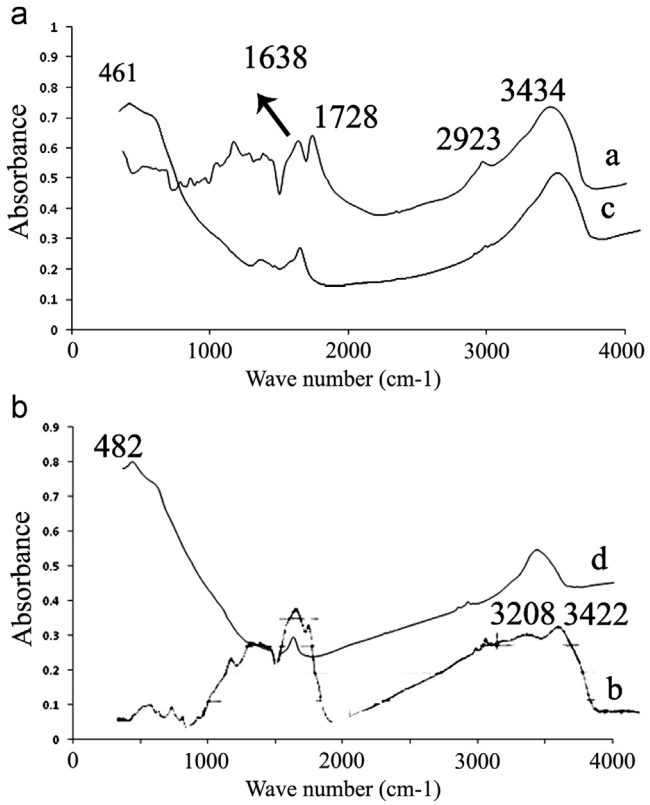

Fig. 9. FTIR spectra of the precursor and the as-synthesized product: (a) gel prepared in acidic medium; (b) gel prepared in alkali medium; and (c and d) corresponding calcined powder at 700 °C.

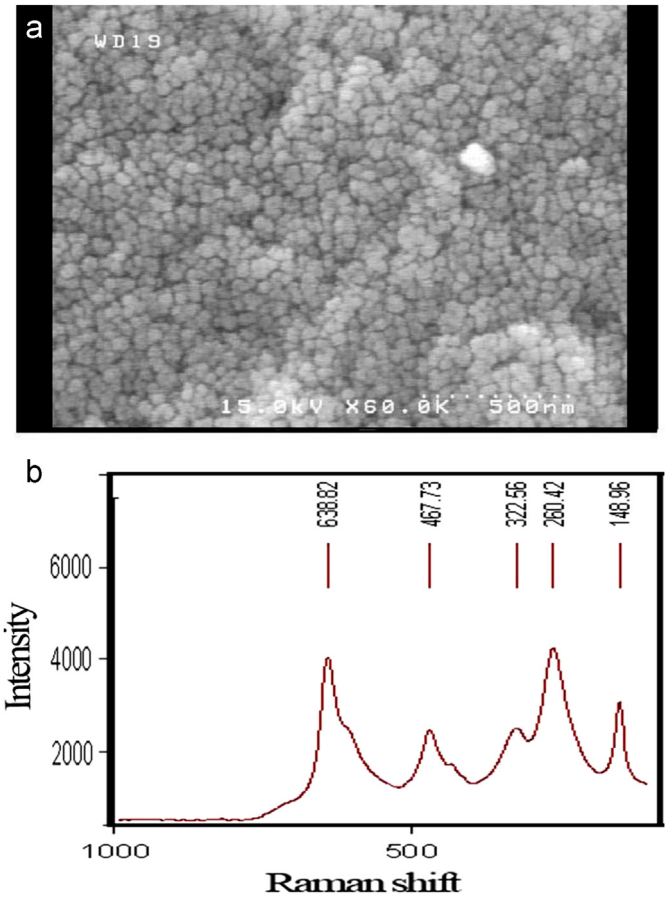

Fig. 10. SEM (a) image and (b) Raman spectra of large scale synthesis of SYDZ nanopowders.

phases of ZrO_2 were expected to have 10 ($5A_u+5B_u$), 3 ($1A_{2u}+2E_u$) and 1 (F_{1u}) IR active modes, respectively [3,4]. The 442–462 cm^{-1} band in SYDZ sample was the distinctive band of tetragonal phase [3,48]. Moreover, the presence of m-ZrO_2 could be ruled out based on the absence of ten active modes of m-phase ($5A_u+5B_u$) peaks between 400 and 745 cm^{-1} [49–52].

The elemental analysis (CHNOS analysis) of the as-prepared sample showed that 0.433wt% carbon existed in the sample. So, this amount of carbon cannot be related to the sample holder or the coating of the samples with conductive layers. The presence of a small amount of carbon in the as-obtained SYDZ samples (corresponding to the residual citric acid) prevents nanocrystals from being agglomerated due to the steric hindrance [18,19,39].

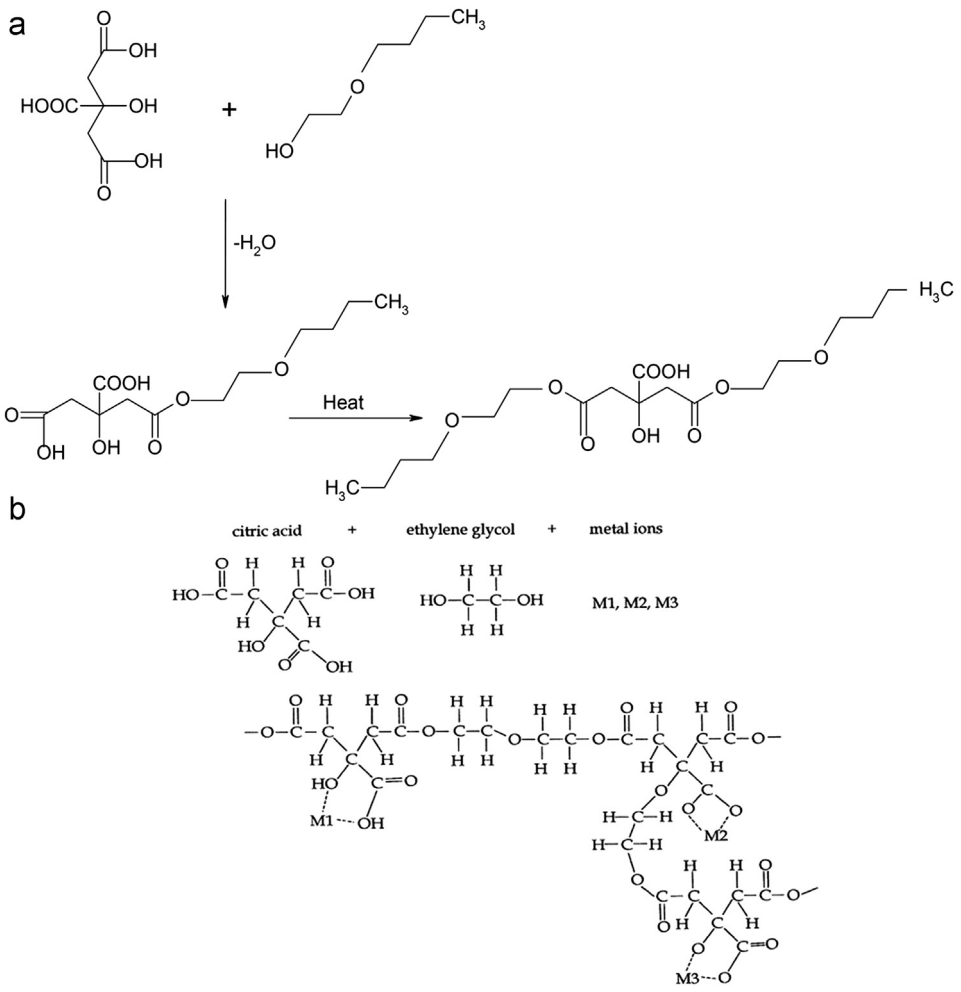

Scheme 1. Schematic diagram of probable mechanism of the modified Pechini method (a)and the conventional Pechini method (b).

3.6. Hypothetical mechanism

There are many works that synthesize rare earth stabilized zirconia with conventional Pechini (polymeric) route [3,19,20,34,35] groups. As previously mentioned, in Robert works, CA:EG (ethylene glycol) mole ratios varied from 0.6 to 2.4 to obtain YSZ nanopowders with less porosity and agglomerate [33,34]. The optimized CA:EG mole ratio was 2.4 ($1Zr^{4+}$:4.77 CA:4.77EG) and the particle size of the obtained powder was 10–20 nm at a calcination temperature of 325–400 °C for 6 h. In the present work, we obtained small agglomerated particles with less amount of CA and EGM ($1Zr^{4+}$:4CA:4EGM) in comparison to the conventional Pechini method.

There are two conditions that seem to give less particle size and agglomeration degree of the present work in comparison to the conventional Pechini method [4,5,23]. It is important to consider the difference in the molecular size of the complexes. In the present study, the citric acid was used only to complex the metal and no further reaction of polymerization occurred in the remaining reactive carboxylic group. Therefore, the resultant molecule of the complex held straight chains which were shorter (Scheme 1a) than the chains produced by the polymeric precursor technique (Pechini method, Scheme 1b). It was due to subsequent esterification and polymerization existing between the free carboxylic group from citric acid and the free hydroxyl group from ethylene glycol. Also, it was because the EGM molecules possessed one alcoholic hydroxyl functional group (–OH) that could react with (–COOH) groups in one CA molecule (Scheme 1a). On the other hand, in the conventional Pechini method, two hydroxyl functional groups in one EG molecule could react with the three carboxylic acid groups (–COOH) in one CA molecule to form a polyester resin. In the present technique, adding a small amount of organic material ($1Zr^{4+}$:4CA:4EGM) into the initial solution released low volatile gases. The removal of volatile masses during calcinations at elevated temperatures plays a significant role in the variation of crystallite sizes. In the Pechini method, the polymeric distribution and its subsequent removal during thermal treatment are expected to control the particle growth and the final morphologies of the particles. An increase in CA:Zr^{4+} mole ratio from 4:1 (present work) to 4.77:1 (Robert work with the conventional Pechini method) [33,34] resulted in slow decomposition of the salts and incomplete combustion of the CA–metal complexes. Thus, a lot of carbonaceous matters were left in the as-prepared powder. During calcinations, the removal of gaseous products from the precursor gave

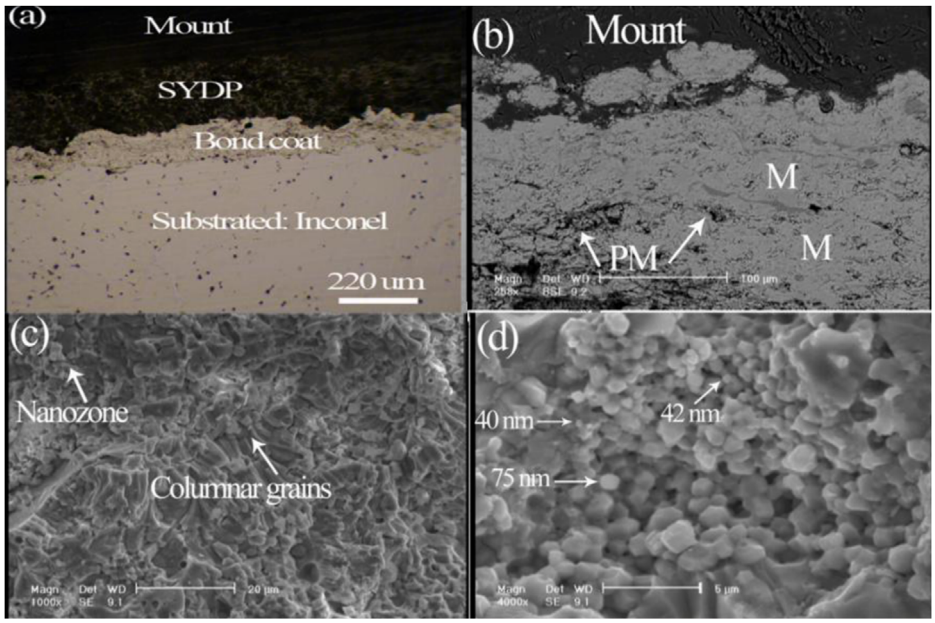

Fig. 11. Optical image (a) and SEM image of polished (b) and fractured (c and d) cross section of APS coating.

rise to capillary forces on the particles, which caused more particles to come in contact with each other. This resulted in more particle agglomeration, cluster formation and particle growth during the synthesis. Thus, there was an increase in particle size with the CA content.

Furthermore, an increase in EGM:Zr^{4+} content from 1.2:1 to 4:1 resulted in a larger separation (more diffusion distance) among the SYDZ particles. In this case, the presence of an excess of citric acid played the role of a space-filling template and the SYDZ particles embedded in polymer matrix became crystalline without interacting with other YSZ particles. This increase in the diffusion distance seemed to be the actual reason for the decrease in the crystallite size upon further increase in citric acid content from 1.2:1 to 4:1 [26,39].

The main function of citric acid and EGM was to provide shorter straight chains in comparison to the conventional Pechini method to hinder cations mobility, which maintained local stoichiometry of unwanted phase. Increasing Zr^{4+}:EGM:CA mole ratios from 1:1.2:1 to 1:4:4 resulted in more –COOH, –OH group and straight chains. The former (EGM) stabilized CA–metal complex and improved the uniformity and metal element in the solution, while the latter (CA) increased potential heat of combustion produced during calcinations [26]. Furthermore, an excess amount of EGM could act as the capping agent and help reduce the crystal size of SYDZ samples.

3.7. Large scale synthesis of SYDZ nanopowders

According to the SEM, TEM, XRD analyses, the optimized specimen, having a low level of agglomerated nanocrystals, was obtained with 1Zr^{4+}:4EGM:4CA mole ratio and pH ~1. In the eventual industrialization of process, a study of synthesis in large scale was undertaken. Two experimental procedures were performed. In the first one, 12 g and in the second, 100 g $ZrO(Cl)_2$ was used. In both experiments, the mole ratio of Zr^{4+}:EGM:CA, equal to 1:4:4, was selected based on our previous results (due to the less particle size and less agglomeration degree of this preparation condition). A scale factor of 4 and then 33 was applied for the quantity of precursors. Using standard synthesis showed that the obtained nanopowders were 3.3 g and 40 g. Fig. 10a shows the SEM of SYDZ nanocrystals prepared from the scale factor of 33. The X-ray diffraction patterns of these samples were the same as experimental results (Fig. 2c). The tetragonal structure of SYDZ nanocrystal was obtained in each case and there was no phase decomposition. Also, no major variation was observed for the grain size. Fig. 10b shows the Raman spectra of large scale product prepared with 1TM:4CA:4EGM. The six peaks centered at 148.96, 260.42, 322.80, 322.56, 467.73 and 638.82 cm^{-1}, confirming that the pure tetragonal phase of as-obtained SYDZ was obtained [44,48].

3.8. Microstructure of APS coating

In addition to bulk samples, the study of nanostructured materials has been extended to coatings processed using the thermal spray technique. In order to spray nanoparticles, the nanosized SYDZ particles are agglomerated via spray-drying (and then sintered) into microscopic particles. Then, these agglomerated nanoparticles were deposited on the Ni-based super alloy via the plasma spraying method. Optical images (Fig. 11a) of polished cross section of coatings showed that the thickness of the bond coat was 100 ± 25 μm, and it was 220–240 μm for the top coat. Fig. 11c shows FESEM micrographs of the fractured cross section of coating obtained from SYDZ granules. The coatings displayed the typical microstructure of

APS coatings deposited from nanostructured powders as used here [18]. The literature indicates that such coating microstructures basically comprise two clearly differentiated zones, yielding a two-scale structure [18]. One coating region, which was completely melted (marked M in Fig. 11b), consisted mainly of submicrometre-sized grains of SYDZ. The other coating region, which was only partly melted (marked PM), largely retained the microstructure of the starting nanopowder, thus principally making up nanometre-sized grains of SYSZ (nanozone). The particle size of this splat-quenched SYSZ is extremely small (20–70 nm, Fig. 11d). Moreover, fractured cross-section of both coatings showed that splats had microcolumnar-grain structure. This columnar structure was formed by directional solidification at rapid cooling [18].

4. Conclusions

The SYDZ nanocrystals were synthesized using the citric acid gel preparation method. In this approach, ethylene glycol monobutyl ether and water were used as the solvent agents. The most important advantage of this method was the decrease in particle size and the reaction time as compared with the conventional ones. The optimized specimen, having a low degree of agglomerated nanocrystals, was obtained with Zr^{4+}:EGM:CA mole ratio 1:4:4 at pH = ~1. This sample contained semispherical particles and the medium particles and crystallite size were between 24 and 34 nm, and 15 ± 2 nm, respectively. Raman, SAED and FTIR analyses assured that non-transformable tetragonal SYDZ nanocrystals were obtained by the modified Pechini method at Sc_2O_3:Y_2O_3 mole ratio equal to 3.6:0.4. The SYDZ powder plasma sprayed well, and produced adherent coating which was essentially 100% tetragonal.

Acknowledgment

The authors would like to acknowledge Malek Ashtar University of Technology, Department of material engineering, for the financial support. One of the authors would like to thank Dr. F. Karimzadeh for allowing us to work in their laboratory. This work is dedicated to Sara, the first author's daughter.

References

[1] M. Salavati-Niasari, M. Dadkhah, F. Davar, Synthesis and characterization of pure cubic zirconium oxide nanocrystals by decomposition of bis-aqua, tris-acetylacetonato zirconium(IV) nitrate as new precursor complex, Inorganica Chimica Acta 362 (2009) 3969–3974.

[2] R.L. Jones, Phase stability of scandia–yttria-stabilized zirconia TBCs, Surface and Coatings Technology 108–109 (1998) 107–113.

[3] S. Farhikhteh, A. Maghsoudipour, B. Raissi, Synthesis of nanocrystalline YSZ (ZrO_2–$8Y_2O_3$) powder by polymerized complex method, Journal of Alloys and Compounds 491 (2010) 402–405.

[4] F. Heshmatpour, R. Babadi-Aghakhanpour, Synthesis and characterization of superfine pure tetragonal nanocrystalline sulfated zirconia powder by a non-alkoxide sol–gel route, Advanced Powder Technology 23 (2012) 80–87.

[5] H. Edris, R. Shoja Razavi, M. Loghman, synthesis of scandia, yttria stabilized zirconia via new wet chemistry method, Current Nanoscience 8 (2012) 767–775.

[6] V.V. Lakshmi, R. Bauri, S. Paul, Effect of fuel type on microstructure and electrical property of combustion synthesized nanocrystalline scandia stabilized zirconia, Materials Chemistry and Physics 126 (2011) 741–746.

[7] R.L. Jones, D. Mess, Scandia, yttria-stabilized zirconia for thermal barrier coatings, Surface and Coatings Technology 82 (1996) 70–76.

[8] R. Shoja Razavi, H. Edris, synthesis and characterization of cubic scandia stabilized zirconia via new wet chemisty method, Current Nanoscience 8 (2012) 807–812.

[9] M. Salavati-Niasari, M. Dadkhah, F. Davar, Pure cubic ZrO_2 nanoparticles by thermolysis of a new precursor, Polyhedron 28 (2009) 3005.

[10] H. Huang, C.-H. Hsieh, N. Kim, J. Stebbins, F. Prinz, Structure, local environment, and ionic conduction in scandia stabilized zirconia, Solid State Ionics 179 (2008) 1442–1445.

[11] S. Wang, F. Zhao, L. Zhang, F. Chen, Synthesis of $BaCe_{0.7}Zr_{0.1}Y_{0.1}Yb_{0.1}O_{3-\delta}$ proton conducting ceramic by a modified Pechini method, Solid State Ionics 213 (2012) 29–35.

[12] T.L. Politova, J.T.S. Irvine, Investigation of scandia–yttria–zirconia system as an electrolyte material for intermediate temperature fuel cells-influence of Yttria content in system $(Y_2O_3)_x(Sc_2O_3)_{11-x}(ZrO_2)_{89}$, Solid State Ionics 168 (2004) 153–165.

[13] R.L. Jones, Some aspects of the hot corrosion of TBCs, Journal of Thermal Spray Technology 6 (1997) 77–84.

[14] J. Jang, K. Dae-Joon, D.Y. Lee, Unusual calcination temperature dependent tetragonalal monoclinic transitions in rare earth-doped zirconia nanocrystals, Journal of Materials Science 36 (2001) 5391.

[15] S.K. Tiwari, J. Adhikary, T.B. Singh, R. Singh, Preparation and characterization of sol–gel derived yttria doped zirconia coatings on AISI 316L, Thin Solid Films 517 (2009) 4502–4508.

[16] M. Gaudon, Ch. Laberty-Robert, F. Ansart, P. Stevens, Thick YSZ films prepared via a modified sol–gel route: thickness control, Journal of the European Ceramic Society 26 (2006) 3153–3160.

[17] M.R Loghman-Estarki, R. Shoja Razavi, H. Edris, Synthesis and thermal stability of ZrO_2, Re = Sc, Y nanocrystals, Defect and Diffusion Forum 334 (2013) 60.

[18] H. Jamali, R. Mozafarinia, R. Shoja Razavi, R. Ahmadi-Pidani, M. R. Loghman-Estarki, Fabrication and evaluation of plasma-sprayed nanostructured and conventional YSZ thermal barrier coatings, Current Nanoscience 8 (2012) 402.

[19] Y.W. Zhang, A. Li, Z. Yan, G. Xu, C. Liao, C. Yan, $(ZrO_2)_{0.85}$-$(REO_{1.5})_{0.15}$ (RE = Sc, Y) solid solutions prepared via three Pechini-type gel routes: 1—gel formation and calcination behaviors, Journal of Solid State Chemistry 171 (2003) 434–438.

[20] Y.W. Zhang, Z.G Yan, F.H. Liao, C.S. Liao, C.H. Yan, Citrate gel synthesis and characterization of $(ZrO_2)_{0.85}(REO_{1.5})_{0.15}$ (RE $_{1/4}$ Y, Sc) solid solutions, Materials Research Bulletin 39 (2004) 1763–1777.

[21] C. Viazzi, A. Deboni, J.Z. Ferreira, J.P. Bonino, F. Ansart, Synthesis of yttria stabilized zirconia by sol–gel route: influence of experimental parameters and large scale production, Solid State Sciences 8 (2006) 1023–1028.

[22] S. Sakka, H. Kozuka, Handbook of Sol–Gel Science and Technology Processing, Characterization and Applications, 2nd ed., Kluwer Academic Publishers, Boston, 60–76.

[23] M. Hajizadeh Oghaz, R. Shoja Razavi, M.R. Loghman-Estarki, R. Ghasemi, Optimization of morphology and particle size of modified sol gel synthesized YSZ Nano powder using Taguchi Method, Journal of Nano Research 21 (2013) 65.

[24] G.H Stout, L.H. Jensen, X-Ray Structure Determination, 2nd edition, John Wiley and Sons, New York, 1989.

[25] Z. Lei, Q. Zhu, S. Zhang, Nanocrystalline scandia-doped zirconia (ScSZ) powders prepared by a glycine–nitrate solution combustion route, Journal of the European Ceramic Society 26 (2006) 397–401.

[26] K.A. Singh, L.C. Pathak, S.K. Roy, Effect of citric acid on the synthesis of nano-crystalline yttria stabilized zirconia powders by nitrate–citrate process, Ceramics International 33 (2007) 1463–1468.

[27] G.C.C. Costa, R. Muccillo, Comparative studies on properties of scandia-stabilized zirconia synthesized by the polymeric precursor and the polyacrylamide techniques, Journal of Alloys and Compounds 503 (2010) 474–479.
[28] Teragonal, JSPDS no. 01-071-1284, Zirconium Scandium Oxide (2000).
[29] R. Srinivasan, R.J. De Angelis, G. Ice, B.H. Davis, Identification of tetragonal and cubic structures of zirconia using synchrotron x-radiation source, Journal of Materials Research 6 (1991) 1287–1291.
[30] K.K. Srivastava, R.N. Patil, C.B. Choudhary, K.V.G.K. Gokhale, E.C. Subba Rao, Martensitic transformation in zirconia, Transactions and Journal of the British Ceramic Society 73 (1974) 85–91.
[31] M. Dapiaggi, F. Magli, Il. Tredici, B. Maroni, G. Borghini, Umberto A. Tamburini, Complex thermal evolution of size-stabilized tetragonal zirconia, Journal of Physics and Chemistry of Solids 71 (2010) 1038–1041.
[32] Ch.L. Robert, F. Ansart, C. Deloget, M. Gaudon, A. Rousset, Powder synthesis of nano crystalline ZrO_2–8%Y_2O_3 via a polymerziation route, Materials Research Bulletin 36 (2001) 2083–2101.
[33] Ch.L. Robert, F. Ansart, S. Castillo, G. Richard, Synthesis of YSZ powders by the Sol–Gel method: surfactant effects on the morphology, Solid State Sciences 4 (2002) 1053–1059.
[34] M. Rezaei, S.M. Alavi, S. Sahebdelfar, Z.F. Yan, Synthesis of ceria doped nanozirconia powder by a polymerized complex method, Journal of Porous Materials 6 (2009) 497–505.
[35] R.C. Garvie, R.H. Hannink, R.T. Pascoe, Phase analysis in zirconia systems, Nature 258 (1975) 703–704.
[36] V.B. Kul'met'eva, S.E. Porozova, B.L. Krasnyi, V.P. Tarasovskii, A.B. Krasnyi, preparation of zirconia ceramics from powder synthesized by a sol–gel method, Refractories and Industrial Ceramics 50 (2009) 438.
[37] Y. Xu, X. Yuan, G. Huang, H. Mater, Polymeric precursor synthesis of $Ba_2Ti_9O_{20}$, Chemical Physics 90 (2005) 333–338.
[38] P. Xu, G. Lu, C. Huang, C. Zeng, Synthesis of $La(Mg_{1/2}Ti_{1/2})O_3$ via citric acid precursor, Materials Chemistry and Physics 92 (2005) 220–224.
[39] R. Shoja Razavi, M.R. Loghman-Estarki, M. Farhadi-Khouzani, M Barekat, H. Jamali, Large scale synthesis of zinc oxide nano- and submicro-structure by Pechini's Method: effect of ethylene glycol/citric acid mole ratio on structural and optical properties, Current Nanosciences **7** (2011) 807–812.
[40] H.F. Yu, K.C. Huang, Effects of pH and citric acid contents on characteristics of ester-derived $BaFe_{12}O_{19}$ powder, Journal of Magnetism and Magnetic Materials 260 (2003) 455–461.
[41] D. Thangaraju, P. Samuel, S. Moorthy Babu, Growth of two-dimensional $KGd(WO_4)_2$ nanorods by modified sol–gel Pechini method, Optical Materials 32 (2010) 1321–1324.
[42] Ji Z, Haynes J.A, Ferber M.K, Rigsbee J.M, Metastable tetragonal zirconia formation and transformation in reactively sputter deposited zirconia coatings, Surface and Coatings Technology 135 (2001) 109–117.
[43] R.L. Jones, Scandia, Yttria Stabilized Zirconia for Ultra High Temperatures TBCs, US Patent no. 5, 780, 1998, p. 178.
[44] M. Ishigame, T. Sakurai, Temperature dependence of the Raman spectra of ZrO_2, Journal of the American Ceramic Society 60 (1977) 367–369.
[45] T. Aruna, N. Balaji, K.S. Rajam, Phase transformation and wear studies of plasma sprayed yttria stabilized zirconia coatings containing various mol% of yttria, Materials Characterization 62 (2011) 697–705.
[46] K. Nomura, Y. Mizutani, M. Kawai, Y. Nakamura, O. Yamamoto, Aging and Raman scattering study of scandia and yttria doped zirconia, Solid State Ionics 132 (2000) 235–239.
[47] P. Southon, Structural Evolution During the Preparation and Heating of Nanophase Zirconia Gel, Ph.D. Thesis, Sydney University of Technology, 2000.
[48] C.M. Phillippi, K.S. Mazdiyasni, Infrared and Raman spectra of zirconia polymorphs, Journal of the American Ceramic Society 54 (1971) 254–258.
[49] M. Salavati-niasari, M. Dadkhah, M. Nourani, A. Amini Fazl', Synthesis and characterization of single-phase cubic ZrO_2 spherical nanocrystals by decomposition route, Journal of Cluster Science 23 (2012) 1011–1017.
[50] S. Chen, Y. Yin, D. Wang, Y. Liu, X. Wang, Structures, growth modes and spectroscopic properties of small zirconia clusters, Journal of Crystal Growth 282 (2005) 498–505.
[51] C. Sa´nchez, J. Doria, C. Paucar, M. Hernandez, A. Mo´squera, J.E. Rodrı´guez, A. Go´mez, E. Baca, O. Mora´n, Nanocystalline ZnO films prepared via polymeric precursor method (Pechini), Physica B 405 (2010) 3679–3684.
[52] M. Mohammadikish, F. Davar, M.R. Loghman-Estarki, Controllable synthesis of metastbale tetragonal zirconia nanocrystals using citric acid assisted sol–gel method, Ceramics International 39 (2013) 2933–2941.